Advances in Nano Research, *Vol. 17, No. 6 (2024) 509-523*
https://doi.org/10.12989/anr.2024.17.6.509

Deformation analysis of a sandwich panel containing graphene origami configuration reinforcement

Mohanad Hatem Shadhar[1], Zaid A. Mohammed[2], Mazin Hussien Abdullah[*3], Arak Vora[4], Malatesh Akkur[5], Ankit Kedia[6], Shivender Singh[7], Majed Alsubih[8] and Saiful Islam[8]

[1]*Department of Civil Engineering, College of Engineering, Al-Iraqia University, Baghdad, Iraq*
[2]*Al-Bayan University, Technical college of Engineering, Department of Medical Instrument Technical Engineering, Iraq*
[3]*College of Medical Informatics, University of information and communication technology, Baghdad, Iraq*
[4]*Marwadi University Research Center, Department of Civil Engineering, Faculty of Engineering & Technology, Marwadi University, Rajkot-360003, Gujarat, India*
[5]*Department of Physics & Electronics, School of Sciences, JAIN (Deemed to be University), Bangalore, Karnataka, India*
[6]*NIMS School of Mechanical and Aerospace Engineering, NIMS University Rajasthan, Jaipur, India*
[7]*Department of Mechanical Engineering, Chandigarh College of Engineering, Chandigarh Group of Colleges-Jhanjeri, Mohali-140307, Punjab, India*
[8]*Civil Engineering Department, College of Engineering, King Khalid University, Abha 61421, Saudi Arabia*

(*Received October 7, 2024, Revised November 1, 2024, Accepted November 2, 2024*)

Abstract. Elasto-static analysis of a higher-order mathematically modeled sandwich panel is studied in this paper. The governing equations are derived using virtual work principle. The sandwich panel is assumed composed of graphene nanoplatelets reinforced shell. One can use the rule of mixture and Halpin-Tsai micromechanical model for extension of constitutive relations and presentation of dependent material properties. The solution is obtained using the solution of eigenvalue characteristic equation. The deformation analysis is presented for the clamped boundary conditions. The results are presented to investigate influence of material parameters such as folding, volume fraction and some other parameters on the deformation responses of the reinforced cylindrical panel.

Keywords: deformation analysis; energy method; graphene origami; higher order kinematic modeling; nanoplatelets

1. Introduction

Foldable materials and structures are introduced as a novel option for application in engineering structures and tuneable materials. Suggestion of novel material with tuneable material properties and providing a controllable range for changing the material properties is a new challenge for material and engineering scientist (Wang *et al*. 2020, 2023, 2024a, b, Feng *et al*. 2024). Manufacturing the composite and hybrid materials and structures offers a new option for controllable material and structures (Liu *et al*. 2023a, b, 2024, Lei *et al*. 2024, Bai *et al*. 2020). A novel foldable nanocomposite structure composed of copper matrix is introduced in this paper for application in vibrational purpose using a mathematical modeling and some experimental relations for material properties (Xie *et al*. 2024a, b, c, Jing *et al*. 2024, Rui *et al*. 2024).

A novel periodic material in the class of metamaterials made of three-phase composition was suggested by Zhu and iong (2023). Application and high range of controllable material properties in origami based material and structure was suggested by Ho *et al*. (2020) for providing an extended range of thermal expansion property. A positive/ negative range for mentioned material property was found in this work. The interesting material properties of folding process and hydrogenation were described for manufacturing of 3D nanostructures by Lv *et al*. (2014) which leads to a wide range for change of photonic/thermal/mechanical/ electrical properties (Yang *et al*. 2024, Zhen *et al*. 2024, Dong *et al*. 2023, 2024). Application of foldable nano-structures was developed in solar-based generators with energy absorption properties by Hong *et al*. (2018). There are some important works on the foldable structures and materials in the literature (Liu *et al*. 2023a, Zhao *et al*. 2022, 2023, 2024a, b). Zhu and Li (2014) explained the hydrogenation process in nano manufacturing and nano building of the new controllable shapes named as graphene origami in which the folding degree can use as a novel parameter in controlling the effective material properties. They illustrated significant importance of various nano-structures patterns and arriving the novel tunable material properties using the molecular dynamic simulations (Zhang *et al*. 2023a, b, 2024a, b, c). Shenoy and Gracias (2012) reported an extended review on the self-folding thin films from nano polyhedral to graphene (Zhan *et al*. 2024, Zhu *et al*. 2024, Fan *et al*. 2024 a, b). Researchers tried to provide some new formulations for analysis of plates and shell with more efficient mathematical operations. Kuang *et al*. (2018) applied thermodynamic extremal principle to diffusion-controlled phase transformations in Fe-C-X alloys. Du *et al*. (2022) developed application of nano graphite film in

*Corresponding author, Ph.D.,
E-mail: science.emk@gmail.com

ISSN: 2287-237X (Print), 2287-2388 (Online)

dynamic of photo excited hot carrier. There are some important references for the basic relations in the literature.

Ho *et al*. (2020) summarized a report on the flexibility and auxeticity of graphene origami metamaterials. They confirmed the analysis using the simulation based on molecular dynamic. It was concluded that using application of large strain, one can receive auxeticity in compressive and tensile regimes. Mu *et al*. (2015) introduced applications of graphene origami to overcome the limitations of polymer materials such as slow reflections. In this work authors suggested a graphene oxide as a building block in nano scale. The self-folding property may suggest a wide range for application in robotics, artificial muscles and also sensing operations. Zhang *et al*. (2023a) introduced a new two dimensional material named as origami for application in various technical areas such as sensor, intelligent and electronic devices. Using some novel experiments, the kinetics and dynamics of graphene was explored at the atomic levels. An *et al*. (2023) studied buckling and bending responses of irregular plates reinforced with graphene origami based on higher order shear deformation theory. The plate was included some holes and the effective material properties were estimated through micromechanical models. The governing equations derived using principle of virtual work was solved using generalized finite difference method, meshless and Taylor series expansion. Energy saving application of photonic materials was developed by Araki and Zhang (2021, 2021). Costa *et al*. (2013) developed application of graphene origami like structures in spintronic applications. Wei *et al*. (2020) explained a new method to tailor graphene sheets into specified pieces and also extension of folding process of graphene into various geometric configurations. Samaniego *et al*. (2020) developed importance of powerful methods such as mesh free and isogeometric analysis for solution of the partial differential equations. Authors explored deep neural network as a new option for function approximation machines. Zhuang *et al*. (2021) developed an energy method based on deep autoencoder for studying the buckling, bending and vibration analysis of plate using the Kirchhoff hypothesis. The objective function is to minimize the total potential energy. For the vibration and buckling analysis, the loss function is constructed based on Rayleigh's principle and the fundamental frequency and the critical buckling load is extracted. Guo *et al*. (2019) studied application of deep collocation method for analysis of a thin plate. A combination of optimizers is adopted in the backpropagation process to minimize the loss function so as to obtain the optimal hyperparameters. Some works on the new materials are available in Yu *et al*. 2021, 2024a, b, 2025, Bao *et al*. 2025. There are some material composition and characteristics in the recent paper (Chen *et al*. 2023, 2024, Wu *et al*. 2023, 2024 a, b). The detection systems can be used from the novel materials (Ren *et al*. 2024, Huang *et al*. 2022, 2024a, b, Tian *et al*. 2024).

A review on the foldable capability of nanostructures and nanocomposites was explained with focus on the mechanical, thermal and electrical properties of graphene origami as a tuneable and controllable material and structure (Bai *et al*. 2022, 2023, 2024a, b, c). One can arrive this conclusion that these materials can be used in various situations such as thermal and mechanical environment for static and dynamic behaviors (Li *et al*. 2023, 2024a, b, Guo *et al*. 2023, 2024). The behavioral relations are extended in the curved system of coordinate using the experimental/ statistical relations from the valid sources. The vibrational characteristics of the shell made of graphene origami is studied in this paper using a shear deformable model. The sensitivity of vibrational characteristics to the thermal loads, foldability and origami content is examined and the impact of each parameter is studied on the responses.

2. Formulation

The mathematical modelling is presented in this section. The model is composed of a porous core with thickness h_c and two graphene origami reinforced face-sheets with thickness h_f. The panel has length L, mean radius R and span angle ϕ.

The material and location dependent density, and modulus of elasticity are presented in Eq. 1 for various distributions (A: Monotonous type, B: Symmetric type, C: Nonsymmetric type) as follows:

$$\begin{gathered} Type\ A: E_c(Z) = E_0\ (1-e_0), \rho_c(Z) = \rho_0\ (1-e_0) \\ Type\ B: E_c(Z) = E_0\ \left[1 - e_0 \cos\left(\frac{\pi z}{h_c}\right)\right], \\ \rho_c(Z) = \rho_0\ \left[1 - e_0 \cos\left(\frac{\pi z}{h_c}\right)\right] \\ Type\ C: E_c(Z) = E_0\ \left[1 - e_0 \cos\left(\frac{\pi z}{h_c} + \frac{\pi}{4}\right)\right], \\ \rho_c(Z) = \rho_0\ \left[1 - e_0 \cos\left(\frac{\pi z}{h_c} + \frac{\pi}{4}\right)\right] \end{gathered} \tag{1}$$

The effective material properties of graphene origami reinforced face-sheets are defined as follows (Fu *et al*. 2023, Jia *et al*. 2024, Jiang *et al*. 2024, Liang *et al*. 2024, Lu *et al*. 2025):

$$\begin{gathered} E_f = \frac{1+\xi\eta V_{Gr}}{1-\eta V_{Gr}} E_{Cu} \times f_E(H_{Gr}, V_{Gr}, T), \\ \rho_f = (\rho_{Gr} V_{Gr} + \rho_{cu} V_{cu}) \times f_\rho(V_{Gr}, T), \\ \nu_f = (\nu_{Gr} V_{Gr} + \nu_{cu} V_{cu}) \times f_\nu(H_{Gr}, V_{Gr}, T) \end{gathered} \tag{2}$$

In which, $V_{Gr} = \frac{\rho_{Cu} W_{Gr}}{\rho_{Cu} W_{Gr} + \rho_{Gr}(1-W_{Gr})}$, $V_{Cu} = 1 - V_{Gr}$, $\xi = 2\frac{l_{Gr}}{t_{Gr}}$, $\eta = \frac{\frac{E_{Gr}}{E_{cu}} - 1}{\frac{E_{Gr}}{E_{cu}} + \xi}$ are defined in terms of graphene origami characteristics such as l_{Gr}, t_{Gr}. The graphene origami may be dispersed along the thickness direction with various distributions including:

Uniform distribution (U_W_{Gr})

$$V_{Gr}(Z) = V_{Gr} \tag{3}$$

$$\begin{gathered} V_{Gr}(Z) = \frac{2V_{Gr}|2K - N_L - 1|}{N_L}, \\ N_L = Number\ of\ layers \end{gathered} \tag{4}$$

Various folding distribution are classified as follows:
Uniform distribution (U_H_{Gr}):

$$H_{Gr}(Z) = H_{Gr} \tag{5}$$

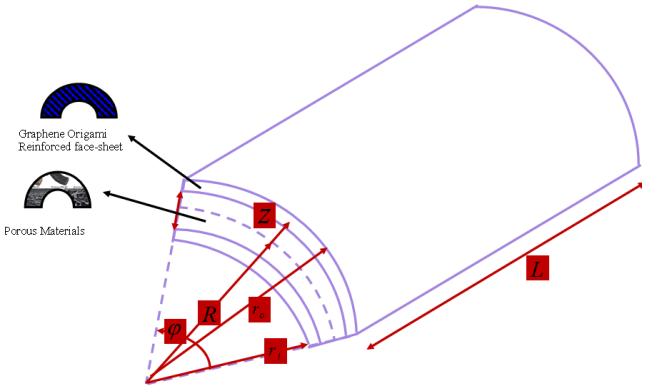

Fig. 1 The schematic figure of a cylindrical composite panel

Non-uniform distribution (X_H_{Gr})

$$H_{Gr}(Z) = H_{Gr}cos(\frac{Z}{h}\pi) \tag{6}$$

The modifier coefficients f_E, f_ρ, f_ν are assumed as follows:

$$f_E(H_{Gr},V_{Gr},T) = 1.11 - 1.22V_{Gr} - 0.134\left(\frac{T}{T_0}\right) + 0.559V_{Gr}\left(\frac{T}{T_0}\right) - 5.5H_{Gr}V_{Gr} + 38H_{Gr}V_{Gr}^2 - 20.6H_{Gr}^2V_{Gr}^2 \tag{7}$$

$$f_\nu(H_{Gr},V_{Gr},T) = 1.01 - 1.43V_{Gr} - 0.165\left(\frac{T}{T_0}\right) + 1.1H_{Gr}V_{Gr}\left(\frac{T}{T_0}\right) - 16.8H_{Gr}V_{Gr} + 16H_{Gr}^2V_{Gr}^2 \tag{8}$$

$$f_\rho(V_{Gr},T) = 1.01 - 2.01V_{Gr}^2 - 0.0131\left(\frac{T}{T_0}\right) \tag{9}$$

In which T is the environment temperature and T_0 is reference temperature. It is assumed that the reinforcements are dispersed along the thickness direction and no changes at a defined transverse direction is observed. No concentration and agglomeration of the nanocomposite reinforcements is considered in our assumptions.

The displacement components are extended as (Ling *et al*. 2024, Hu *et al*. 2024, Hui *et al*. 2023, Cheng *et al*. 2024, Tian *et al*. 2024):

$$\{u,v,w\} = \{u_0,v_0,w_0\} + z\{\theta_1,\theta_2,\xi_1\theta_3\} + z^2\{u_1,v_1,\xi_2u_1\} + z^3\{\phi_1,\phi_2,\phi_3\} \tag{10}$$

Based on Eq. (10), it is assumed that the displacements are changed along the thickness direction using the third-order function that leads to more accurate formulation and analysis. Using the higher-order modelling, the strain components are derived as follows (Sun *et al*. 2024):

$$\varepsilon_x = u_{0,x} + z\theta_{1,x} + z^2u_{1,x} + z^3\varphi_{1,x}$$
$$\varepsilon_\varphi = \frac{1}{R}\begin{Bmatrix} v_{0,\varphi} + w_0 + z(\theta_{2,\varphi} + \theta_3) \\ +z^2(v_{0,\varphi} + w_0) + z^3(\phi_{2,\varphi} + \phi_3) \end{Bmatrix}$$
$$\varepsilon_z = \theta_3 + 2zw_0 + z^2 3\phi_3$$
$$\gamma_{xz} = w_{0,x} + \theta_1 + z(\theta_{3,x} + 2u_1) + z^2(w_{0,x} + 3\phi_1) + z^3\phi_{3,x}$$
$$\gamma_{\varphi z} = \frac{1}{R}\begin{Bmatrix} w_{0,\varphi} + R\theta_2 - v_0 + z(\theta_{3,\varphi} + 2Rv_1) \\ +z^2(w_{0,\varphi} + 3R\phi_2 + v_1) + z^3(\phi_{3,\varphi} + 2\phi_2) \end{Bmatrix}$$
$$\gamma_{x\phi} = v_{0,x} + z\theta_{2,x} + z^2v_{1,x} + z^3\phi_{2,x} \tag{11}$$

The thermal strain included relations are developed as (Zhou *et al*. 2020, Kadiri *et al*. 2024, Sekkak *et al*. 2024, Dai *et al*. 2021)

$$\begin{bmatrix}\sigma_x\\ \sigma_\varphi\\ \sigma_z\\ \tau_{x\varphi}\\ \tau_{xz}\\ \tau_{\varphi z}\end{bmatrix} = \frac{E_C(z)}{(1+\upsilon_c)(1-2\upsilon_c)} \begin{bmatrix} 1 & \upsilon_c & \upsilon_c & 0 & 0 & 0 \\ \upsilon_c & 1 & \upsilon_c & 0 & 0 & 0 \\ \upsilon_c & \upsilon_c & 1 & 0 & 0 & 0 \\ 0 & 0 & 0 & \frac{1-2\nu_c}{2} & 0 & 0 \\ 0 & 0 & 0 & 0 & \frac{1-2\nu_c}{2} & 0 \\ 0 & 0 & 0 & 0 & 0 & \frac{1-2\nu_c}{2} \end{bmatrix} \begin{bmatrix}\varepsilon_x\\ \varepsilon_\varphi\\ \varepsilon_z\\ \gamma_{x\varphi}\\ \gamma_{xz}\\ \gamma_{\varphi z}\end{bmatrix} - \frac{\alpha E}{1-2\nu}\begin{bmatrix}\Delta T\\ \Delta T\\ \Delta T\\ 0\\ 0\\ 0\end{bmatrix} \tag{12}$$

The strain energy is extended as (Tlidji *et al*. 2022, Kumar *et al*. 2021, Din *et al*. 2023):

$$U = \frac{1}{2}\begin{Bmatrix} \sigma_x\varepsilon_x + \sigma_\phi\varepsilon_\phi + \sigma_z\varepsilon_z \\ +\tau_{x\phi}\gamma_{x\phi} + \tau_{xz}\gamma_{xz} + \tau_{z\phi}\gamma_{z\phi} \end{Bmatrix} \tag{13}$$

One can arrive strain energy variation as:

$$\begin{aligned}\delta u = \iint\Big(&\left[\frac{\partial N_x}{\partial x} + \frac{1}{R}\frac{\partial N_{x\varphi}}{\partial \varphi}\right]\delta u_0 + \left[\frac{\partial M_x}{\partial x} + \frac{1}{R}\frac{\partial M_{x\varphi}}{\partial \varphi} - Q_x\right]\delta\theta_1 \\ &+\left[\frac{\partial N_x^*}{\partial x} + \frac{1}{R}\frac{\partial N_{x\varphi}^*}{\partial \varphi} - 2S_x\right]\delta u_1 + \left[\frac{\partial M_x^*}{\partial x} + \frac{1}{R}\frac{\partial M_{x\varphi}^*}{\partial \varphi} - 3Q_x^*\right]\delta\phi_1 \\ &+\left[\frac{1}{R}\frac{\partial N_\varphi}{\partial \varphi} + \frac{\partial N_{x\varphi}}{\partial x} + \frac{1}{R}Q_\varphi\right]\delta v_0 + \left[\frac{1}{R}\frac{\partial M_\varphi}{\partial \varphi} + \frac{\partial M_{x\varphi}}{\partial x} + Q_\varphi\right]\delta\theta_2 \\ &+\left[\frac{1}{R}\frac{\partial N_\varphi^*}{\partial \varphi} + \frac{\partial N_{x\varphi}^*}{\partial x} - \frac{1}{R}Q_\varphi^* - 2S_\varphi\right]\delta v_1 + \left[\frac{1}{R}\frac{\partial M_\varphi^*}{\partial \varphi} + \frac{\partial M_{x\varphi}^*}{\partial x} + -3Q_\varphi^* - \frac{2}{R}S_\varphi^*\right]\delta\phi_2 \\ &+\left[\frac{\partial Q_x}{\partial x} + \frac{1}{R}\frac{\partial Q_\varphi}{\partial \varphi} - \frac{1}{R}N_\varphi\right]\delta w_0 + \left[\frac{\partial S_x}{\partial x} + \frac{1}{R}\frac{\partial S_\varphi}{\partial \varphi} - \frac{1}{R}M_\varphi - A\right]\delta\theta_3 \\ &+\left[-\frac{1}{R}N_\varphi^* + \frac{\partial Q_x^*}{\partial x} + \frac{1}{R}\frac{\partial Q_\varphi^*}{\partial \varphi} - 2B\right]\delta w_0^* + \left[-\frac{1}{R}M_\varphi^* + \frac{\partial S_x^*}{\partial x} + \frac{1}{R}\frac{\partial S_\varphi^*}{\partial \varphi} - 3D\right]\delta\theta_3^*\Big)dA\end{aligned} \tag{14}$$

The external work is extended as:

$$W_e = \int\int(f.w)ds = \int_0^\phi\int_0^L(p_ir_i - p_or_o)u_z dx d\phi \tag{15}$$

Substitution of resultant components into governing equations yields as follows:

$$\frac{\partial N_x}{\partial x} + \frac{1}{R}\frac{\partial N_{x\varphi}}{\partial \varphi} = 0 \tag{16}$$

$$\frac{\partial M_x}{\partial x}+\frac{1}{R}\frac{\partial M_{x\varphi}}{\partial \varphi}-Q_x=0$$

$$\delta w_0:\frac{\partial N_x^{\,1}}{\partial x}+\frac{\partial N_{x\varphi}^{\,1}}{R\partial \varphi}-2S_x+q-F_f=0$$

$$\delta \theta_1:\frac{\partial M_x^{\,1}}{\partial x}+\frac{\partial M_{x\varphi}^{\,1}}{R\partial \varphi}-3Q_x^{\,1}=0$$

$$\delta \theta_2:\frac{1}{R}\frac{\partial N_\varphi}{\partial \varphi}+\frac{\partial N_{x\varphi}}{\partial x}+\frac{1}{R}Q_\varphi=0$$

$$\delta \theta_3:\frac{1}{R}\frac{\partial M_\varphi}{\partial \varphi}+\frac{\partial M_{x\varphi}}{\partial x}+Q_\varphi+\frac{h}{2}(q-F_f)=0$$

$$\delta u_1:\frac{\partial N_\varphi^{\,1}}{R\partial \varphi}+\frac{\partial N_{x\varphi}^{\,1}}{\partial x}-\frac{Q_\varphi^{\,1}}{R}-2S_\varphi=0$$

$$\delta v_1:\frac{\partial M_\varphi^{\,1}}{R\partial \varphi}+\frac{\partial M_{x\varphi}^{\,1}}{\partial x}-3Q_\varphi^{\,1}-\frac{2S_\varphi^{\,1}}{R}=0$$

$$\delta w_1:\frac{\partial Q_x}{\partial x}+\frac{\partial Q_\varphi}{R\partial \varphi}-\frac{N_\varphi}{R}+\frac{h^2(q-F_f)}{4}=0$$

$$\delta \theta_2:\frac{\partial S_x}{\partial x}+\frac{\partial S_\varphi}{R\partial \varphi}-\frac{M_\varphi}{R}-A=0$$

$$\delta \phi_2:-\frac{N_\varphi^{\,1}}{R}+\frac{\partial Q_x^{\,1}}{\partial x}+\frac{\partial Q_\varphi^{\,1}}{R\partial \varphi}-2B=0$$

$$\delta \phi_3:-\frac{M_\varphi^{\,1}}{R}+\frac{\partial S_x^{\,1}}{\partial x}+\frac{\partial S_\varphi^{\,1}}{R\partial \varphi}-3D+\frac{h^3(q-F_f)}{8}=0$$

3. Solution

Solution of the governing equations of the static bending analysis using the mathematical method of Eigenvalue Eigenvector is presented here. This solution method is applicable for more general boundary conditions and leads to a novel analytical method than the classic solution based on Navier's technique for simply-supported boundary conditions. Before presentation of the solution procedure, the mathematical formulation is presented in the vector form as follows (Dai *et al*. 2023, Addou *et al*. 2023, Arefi *et al*. 2016, 2019, 2021, Arefi and Rahimi 2011, 2012 a, b, c, Arefi 2018, 2020, Arefi and Zenkour 2017, 2018, 2019):

$$[A]\frac{d^2}{dx^2}\{y\}+[B]\frac{d}{dx}\{y\}+[C]\{y\}=\{F\} \tag{17}$$

In which the components of matrices [A], [B], [C] are presented in Appendix A. These matrices are 8×8 ones according to number of unknown functions. The unknown vector for this problem is assumed as (Lori *et al*. 2021, Arefi and Bidgoli 2019, Adab and Arefi 2020, Adab *et al*. 2022, Zhang *et al*. 2023, Rahimi *et al*. 2012, Mohammadi *et al*. 2019):

$$\{U\}=\{u_0\ \ v_0\ \ w_0\ \ \theta_1\ \ \theta_2\ \ \theta_3\ \ u_1\ v_1\ \ w_1\ \ \phi_1\ \ \phi_2\ \ \phi_3\}^T \tag{18}$$

The vector matrix {F} is calculated as:

$$\{F\}=L\phi\begin{Bmatrix}0\\0\\0\\0\\k\\kz\\kz^2\\kz^3\end{Bmatrix}\qquad k=(p_i r_i-p_o r_o) \tag{19}$$

The solution is assumed as follows:

$$\{y\}=\{y\}_h+\{y\}_p \tag{20}$$

Using the solution as $\{y\}=e^{mx}\{v\}$ and substitution yields:

$$e^{mx}\left[m^2[A]+m[B]+[C]\right]\{v\}=\{0\} \tag{21}$$

In which:

$$|m^2A+mB+C|=0 \tag{22}$$

defines eigenvalues. Final the homogeneous solution is obtained as follows:

$$\{y\}_h=\sum_{i=1}^{16}c_i v_i^j e^{\lambda_i x}\qquad j=(1,2,\dots,8),\ i=(1,2,\dots,16) \tag{23}$$

In which c_i are obtained using boundary conditions. The particular solution is obtained as follows:

$$[C]\{y\}_g=\{F\}\Rightarrow\{y\}_g=[C]^{-1}\{F\} \tag{24}$$

Finally, one can arrive at integration constants using the required boundary condition where in this case, we will obtain for clamped boundary condition.

4. Numerical results and discussion

The numerical results and corresponding discussion are presented in this section. All input material properties defined in the mathematical formulation are listed as follows:

$$\{E_{Gr},E_{Cu},E_0\}=\{929.57,65.79,60\}\text{GPa},$$
$$\{\nu_{Gr},\nu_{Cu},\nu_0\}=\{0.22,0.387,0.25\},$$
$$\{\rho_{Gr},\rho_{Cu},\rho_0\}=\{1.8,8.8,2.707\}\times10^3\frac{kg}{m^3},$$
$$\{\alpha_{Gr},\alpha_{Cu}\}=\{-3.98,16.51\}\times10^{-6}\frac{1}{k},$$
$$\{l_{Gr},t_{Gr}\}=\{83.76,3.4\}10^{-10}m$$

Table 1 Longitudinal variation of radial displacement $\boldsymbol{U_z}$ at various surfaces (z=-h/2,0, h/2)

x/L	z=-h/2	z=0	z=h/2
0	0.0000000	0.0000000	0.0000000
0.025	0.5033125	0.4542597	0.4202659
0.050	1.0066250	0.9085193	0.8405319
0.075	1.5099375	1.3627790	1.2607978
0.100	2.0132500	1.8170387	1.6810638
0.125	2.3837500	2.1514297	1.9904313
0.150	2.7542500	2.4858208	2.2997988
0.175	3.1247500	2.8202119	2.6091663
0.200	3.4952500	3.1546029	2.9185338
0.225	3.5855825	3.2361316	2.9939614
0.250	3.6759150	3.3176603	3.0693890
0.275	3.7662475	3.3991890	3.1448167
0.300	3.8565800	3.4807177	3.2202443
0.325	3.8567475	3.4808689	3.2203842
0.350	3.8569150	3.4810201	3.2205240
0.375	3.8570825	3.4811712	3.2206639
0.400	3.8572500	3.4813224	3.2208038
0.425	3.8835728	3.5050797	3.2427832
0.450	3.9098955	3.5288371	3.2647627
0.475	3.9362183	3.5525944	3.2867422
0.500	3.9625410	3.5763518	3.3087217
0.525	3.9362183	3.5525944	3.2867422
0.550	3.9098955	3.5288371	3.2647627
0.575	3.8835728	3.5050797	3.2427832
0.600	3.8572500	3.4813224	3.2208038
0.625	3.8570825	3.4811712	3.2206639
0.650	3.8569150	3.4810201	3.2205240
0.675	3.8567475	3.4808689	3.2203842
0.700	3.8565800	3.4807177	3.2202443
0.725	3.7662475	3.3991890	3.1448167
0.750	3.6759150	3.3176603	3.0693890
0.775	3.5855825	3.2361316	2.9939614
0.800	3.4952500	3.1546029	2.9185338
0.825	3.1247500	2.8202119	2.6091663
0.850	2.7542500	2.4858208	2.2997988
0.875	2.3837500	2.1514297	1.9904313
0.900	2.0132500	1.8170387	1.6810638
0.925	1.5099375	1.3627790	1.2607978
0.950	1.0066250	0.9085193	0.8405319
0.975	0.5033125	0.4542597	0.4202659
1.000	0.0000000	0.0000000	0.0000000

Table 2 Longitudinal variation of axial displacement $\boldsymbol{U_z}$ at various surfaces (z=-h/2,0, h/2)

x/L	z=-h/2	z=0	z=h/2
0	0.0000000	0.0000000	0.0000000
0.025	0.1313058	0.0095197	-0.1148925
0.050	0.2626115	0.0190393	-0.2297851
0.075	0.3939173	0.0285590	-0.3446776
0.100	0.5252230	0.0380787	-0.4595701
0.125	0.4470485	0.0324110	-0.3911674
0.150	0.3688740	0.0267434	-0.3227648
0.175	0.2906995	0.0210757	-0.2543621
0.200	0.2125250	0.0154081	-0.1859594
0.225	0.1707000	0.0123758	-0.1493625
0.250	0.1288750	0.0093434	-0.1127656
0.275	0.0870500	0.0063111	-0.0761688
0.300	0.0452542	0.0032809	-0.0395974
0.325	0.0352543	0.0025559	-0.0308475
0.350	0.0252544	0.0018309	-0.0220976
0.375	0.0152544	0.0011059	-0.0133476
0.400	0.0052545	0.0003810	-0.0045977
0.425	0.0039409	0.0002857	-0.0034483
0.450	0.0026273	0.0001905	-0.0022988
0.475	0.0013136	0.0000952	-0.0011494
0.500	0.0000000	0.0000000	0.0000000
0.525	-0.0013136	-0.0000952	0.0011494
0.550	-0.0026273	-0.0001905	0.0022988
0.575	-0.0039409	-0.0002857	0.0034483
0.600	-0.0052545	-0.0003810	0.0045977
0.625	-0.0152544	-0.0011059	0.0133476
0.650	-0.0252544	-0.0018309	0.0220976
0.675	-0.0352543	-0.0025559	0.0308475
0.700	-0.0452542	-0.0032809	0.0395974
0.725	-0.0870500	-0.0063111	0.0761688
0.750	-0.1288750	-0.0093434	0.1127656
0.775	-0.1707000	-0.0123758	0.1493625
0.800	-0.2125250	-0.0154081	0.1859594
0.825	-0.2906995	-0.0210757	0.2543621
0.850	-0.3688740	-0.0267434	0.3227648
0.875	-0.4470485	-0.0324110	0.3911674
0.900	-0.5252230	-0.0380787	0.4595701
0.925	-0.3939173	-0.0285590	0.3446776
0.950	-0.2626115	-0.0190393	0.2297851
0.975	-0.1313058	-0.0095197	0.1148925
1.000	0.0000000	0.0000000	0.0000000

In this section, the effect of various parameters such as W_{Gr} and H_{Gr} of graphene, various distributions of porosity and graphene, temperature, circumferential and longitudinal coordinates on the deformation of the composite sandwich cylindrical panel is studied.

In order to present a static bending response, the cylindrical panel is subjected to internal pressure 80 MPa, and external pressure 0.1 MPa. Furthermore, it is assumed

Table 3 Longitudinal variation of radial displacement U_z for uniform and X distributions

x/L	FG-U	FG-X
0	0.0000000	0.0000000
0.025	0.5033125	0.2025833
0.050	1.0066250	0.4051666
0.075	1.5099375	0.6077498
0.100	2.0132500	0.8103331
0.125	2.3837500	0.9594594
0.150	2.7542500	1.1085856
0.175	3.1247500	1.2577119
0.200	3.4952500	1.4068381
0.225	3.5855825	1.4431970
0.250	3.6759150	1.4795558
0.275	3.7662475	1.5159146
0.300	3.8565800	1.5522735
0.325	3.8567475	1.5523409
0.350	3.8569150	1.5524083
0.375	3.8570825	1.5524757
0.400	3.8572500	1.5525431
0.425	3.8835728	1.5631380
0.450	3.9098955	1.5737329
0.475	3.9362183	1.5843278
0.500	3.9625410	1.5949228
0.525	3.9362183	1.5843278
0.550	3.9098955	1.5737329
0.575	3.8835728	1.5631380
0.600	3.8572500	1.5525431
0.625	3.8570825	1.5524757
0.650	3.8569150	1.5524083
0.675	3.8567475	1.5523409
0.700	3.8565800	1.5522735
0.725	3.7662475	1.5159146
0.750	3.6759150	1.4795558
0.775	3.5855825	1.4431970
0.800	3.4952500	1.4068381
0.825	3.1247500	1.2577119
0.850	2.7542500	1.1085856
0.875	2.3837500	0.9594594
0.900	2.0132500	0.8103331
0.925	1.5099375	0.6077498
0.950	1.0066250	0.4051666
0.975	0.5033125	0.2025833
1.000	0.0000000	0.0000000

Table 4 Longitudinal variation of axial displacement U_x for uniform and X distributions

x/L	FG-U	FG-X
0	0.0000000	0.0000000
0.025	0.1313058	0.0558312
0.050	0.2626115	0.1116624
0.075	0.3939173	0.1674936
0.100	0.5252230	0.2233248
0.125	0.4470485	0.1900850
0.150	0.3688740	0.1568452
0.175	0.2906995	0.1236054
0.200	0.2125250	0.0903656
0.225	0.1707000	0.0725816
0.250	0.1288750	0.0547977
0.275	0.0870500	0.0370137
0.300	0.0452542	0.0192421
0.325	0.0352543	0.0149901
0.350	0.0252544	0.0107381
0.375	0.0152544	0.0064862
0.400	0.0052545	0.0022342
0.425	0.0039409	0.0016757
0.450	0.0026273	0.0011171
0.475	0.0013136	0.0005586
0.500	0.0000000	0.0000000
0.525	-0.0013136	-0.0005586
0.550	-0.0026273	-0.0011171
0.575	-0.0039409	-0.0016757
0.600	-0.0052545	-0.0022342
0.625	-0.0152544	-0.0064862
0.650	-0.0252544	-0.0107381
0.675	-0.0352543	-0.0149901
0.700	-0.0452542	-0.0192421
0.725	-0.0870500	-0.0370137
0.750	-0.1288750	-0.0547977
0.775	-0.1707000	-0.0725816
0.800	-0.2125250	-0.0903656
0.825	-0.2906995	-0.1236054
0.850	-0.3688740	-0.1568452
0.875	-0.4470485	-0.1900850
0.900	-0.5252230	-0.2233248
0.925	-0.3939173	-0.1674936
0.950	-0.2626115	-0.1116624
0.975	-0.1313058	-0.0558312
1.000	0.0000000	0.0000000

span angle $\phi = 60^o$, length L = 2 m, mean radius R = 0.6 m, and thickness h = 0.12 m.

In this section, the longitudinal variation of deformation components is presented at various radial surfaces.

Table 1 presents longitudinal variation of radial displacement U_z at various surfaces (z=-h/2,0, h/2). It is deduced that the results are very sharp at both ends because of the existence of clamped boundaries and reflects a

Table 5 Longitudinal variation of radial displacement $\boldsymbol{U_z}$ for various $\boldsymbol{N_L = 2, 3, 4, 5}$

x/L	N_L=2	N_L=3	N_L=4	N_L=5
0	0.0000000	0.0000000	0.0000000	0.0000000
0.025	0.0028136	0.0011626	0.0005585	0.0004572
0.050	0.0056271	0.0023251	0.0011170	0.0009144
0.075	0.0084407	0.0034877	0.0016755	0.0013716
0.100	0.0112542	0.0046502	0.0022340	0.0018288
0.125	0.0124053	0.0051259	0.0024624	0.0020159
0.150	0.0135564	0.0056015	0.0026909	0.0022029
0.175	0.0147074	0.0060771	0.0029194	0.0023900
0.200	0.0158585	0.0065527	0.0031479	0.0025770
0.225	0.0163834	0.0067696	0.0032521	0.0026623
0.250	0.0169083	0.0069865	0.0033563	0.0027476
0.275	0.0174331	0.0072034	0.0034605	0.0028329
0.300	0.0179580	0.0074202	0.0035647	0.0029182
0.325	0.0180326	0.0074511	0.0035795	0.0029303
0.350	0.0181072	0.0074819	0.0035943	0.0029424
0.375	0.0181817	0.0075127	0.0036091	0.0029545
0.400	0.0182563	0.0075435	0.0036239	0.0029666
0.425	0.0183554	0.0075844	0.0036435	0.0029827
0.450	0.0184544	0.0076254	0.0036632	0.0029988
0.475	0.0185535	0.0076663	0.0036829	0.0030149
0.500	0.0186525	0.0077072	0.0037025	0.0030310
0.525	0.0185535	0.0076663	0.0036829	0.0030149
0.550	0.0184544	0.0076254	0.0036632	0.0029988
0.575	0.0183554	0.0075844	0.0036435	0.0029827
0.600	0.0182563	0.0075435	0.0036239	0.0029666
0.625	0.0181817	0.0075127	0.0036091	0.0029545
0.650	0.0181072	0.0074819	0.0035943	0.0029424
0.675	0.0180326	0.0074511	0.0035795	0.0029303
0.700	0.0179580	0.0074202	0.0035647	0.0029182
0.725	0.0174331	0.0072034	0.0034605	0.0028329
0.750	0.0169083	0.0069865	0.0033563	0.0027476
0.775	0.0163834	0.0067696	0.0032521	0.0026623
0.800	0.0158585	0.0065527	0.0031479	0.0025770
0.825	0.0147074	0.0060771	0.0029194	0.0023900
0.850	0.0135564	0.0056015	0.0026909	0.0022029
0.875	0.0124053	0.0051259	0.0024624	0.0020159
0.900	0.0112542	0.0046502	0.0022340	0.0018288
0.925	0.0084407	0.0034877	0.0016755	0.0013716
0.950	0.0056271	0.0023251	0.0011170	0.0009144
0.975	0.0028136	0.0011626	0.0005585	0.0004572
1.000	0.0000000	0.0000000	0.0000000	0.0000000

Table 6 Longitudinal variation of axial displacement $\boldsymbol{U_x}$ for various $\boldsymbol{N_L = 2, 3, 4, 5}$

x/L	N_L=2	N_L=3	N_L=4	N_L=5
0	0.0000000	0.0000000	0.0000000	0.0000000
0.025	0.0005813	0.0002779	0.0001769	0.0001011
0.050	0.0011626	0.0005557	0.0003538	0.0002022
0.075	0.0017439	0.0008336	0.0005307	0.0003033
0.100	0.0023252	0.0011114	0.0007076	0.0004044
0.125	0.0020573	0.0009834	0.0006260	0.0003578
0.150	0.0017894	0.0008553	0.0005445	0.0003112
0.175	0.0015214	0.0007272	0.0004630	0.0002646
0.200	0.0012535	0.0005992	0.0003814	0.0002180
0.225	0.0009465	0.0004524	0.0002880	0.0001646
0.250	0.0006394	0.0003056	0.0001946	0.0001112
0.275	0.0003324	0.0001589	0.0001011	0.0000578
0.300	0.0000253	0.0000121	0.0000077	0.0000044
0.325	0.0000221	0.0000105	0.0000067	0.0000038
0.350	0.0000189	0.0000090	0.0000057	0.0000033
0.375	0.0000157	0.0000075	0.0000048	0.0000027
0.400	0.0000125	0.0000060	0.0000038	0.0000022
0.425	0.0000094	0.0000045	0.0000029	0.0000016
0.450	0.0000063	0.0000030	0.0000019	0.0000011
0.475	0.0000031	0.0000015	0.0000010	0.0000005
0.500	0.0000000	0.0000000	0.0000000	0.0000000
0.525	-0.0000031	-0.0000015	-0.0000010	-0.0000005
0.550	-0.0000063	-0.0000030	-0.0000019	-0.0000011
0.575	-0.0000094	-0.0000045	-0.0000029	-0.0000016
0.600	-0.0000253	-0.0000121	-0.0000077	-0.0000044
0.625	-0.0000157	-0.0000075	-0.0000048	-0.0000027
0.650	-0.0000189	-0.0000090	-0.0000057	-0.0000033
0.675	-0.0000221	-0.0000105	-0.0000067	-0.0000038
0.700	-0.0000253	-0.0000121	-0.0000077	-0.0000044
0.725	-0.0003324	-0.0001589	-0.0001011	-0.0000578
0.750	-0.0006394	-0.0003056	-0.0001946	-0.0001112
0.775	-0.0009465	-0.0004524	-0.0002880	-0.0001646
0.800	-0.0012535	-0.0005992	-0.0003814	-0.0002180
0.825	-0.0015214	-0.0007272	-0.0004630	-0.0002646
0.850	-0.0017894	-0.0008553	-0.0005445	-0.0003112
0.875	-0.0020573	-0.0009834	-0.0006260	-0.0003578
0.900	-0.0023252	-0.0011114	-0.0007076	-0.0004044
0.925	-0.0017439	-0.0008336	-0.0005307	-0.0003033
0.950	-0.0011626	-0.0005557	-0.0003538	-0.0002022
0.975	-0.0005813	-0.0002779	-0.0001769	-0.0001011
1.000	0.0000000	0.0000000	0.0000000	0.0000000

uniform distribution at middle surface of the cylindrical panel. Furthermore, one can see that the maximum U_z is occurred at external layer (z= h/2). Table 2 presents longitudinal variation of axial displacement U_x at various surfaces (z=-h/2,0, h/2). It is concluded that the results are tend to zero at middle surface. The maximum U_x is occurred at near the both ends of the cylindrical panel. Furthermore, one can see that the maximum U_z is occurred

Table 7 Longitudinal variation of radial displacement $\boldsymbol{U_z}$ for various T

x/L	T=50	T=100	T=150
0	0.0000000	0.0000000	0.0000000
0.025	0.5033125	0.5096140	0.5151529
0.050	1.0066250	1.0192279	1.0303059
0.075	1.5099375	1.5288419	1.5454588
0.100	2.0132500	2.0384559	2.0606117
0.125	2.3837500	2.4135946	2.4398277
0.150	2.7542500	2.7887332	2.8190437
0.175	3.1247500	3.1638719	3.1982597
0.200	3.4952500	3.5390105	3.5774758
0.225	3.5855825	3.6304740	3.6699333
0.250	3.6759150	3.7219375	3.7623909
0.275	3.7662475	3.8134009	3.8548485
0.300	3.8565800	3.9048644	3.9473060
0.325	3.8567475	3.9050340	3.9474775
0.350	3.8569150	3.9052036	3.9476489
0.375	3.8570825	3.9053732	3.9478204
0.400	3.8572500	3.9055428	3.9479918
0.425	3.8835728	3.9321951	3.9749338
0.450	3.9098955	3.9588474	4.0018758
0.475	3.9362183	3.9854997	4.0288178
0.500	3.9625410	4.0121520	4.0557598
0.525	3.9362183	3.9854997	4.0288178
0.550	3.9098955	3.9588474	4.0018758
0.575	3.8835728	3.9321951	3.9749338
0.600	3.8572500	3.9055428	3.9479918
0.625	3.8570825	3.9053732	3.9478204
0.650	3.8569150	3.9052036	3.9476489
0.675	3.8567475	3.9050340	3.9474775
0.700	3.8565800	3.9048644	3.9473060
0.725	3.7662475	3.8134009	3.8548485
0.750	3.6759150	3.7219375	3.7623909
0.775	3.5855825	3.6304740	3.6699333
0.800	3.4952500	3.5390105	3.5774758
0.825	3.1247500	3.1638719	3.1982597
0.850	2.7542500	2.7887332	2.8190437
0.875	2.3837500	2.4135946	2.4398277
0.900	2.0132500	2.0384559	2.0606117
0.925	1.5099375	1.5288419	1.5454588
0.950	1.0066250	1.0192279	1.0303059
0.975	0.5033125	0.5096140	0.5151529
1.000	0.0000000	0.0000000	0.0000000

Table 8 Longitudinal variation of radial displacement $\boldsymbol{U_z}$ for various T

x/L	T=50	T=100	T=150
0	0.0000000	0.0000000	0.0000000
0.025	0.1313058	0.1329497	0.1343947
0.050	0.2626115	0.2658994	0.2687894
0.075	0.3939173	0.3988491	0.4031842
0.100	0.5252230	0.5317988	0.5375789
0.125	0.4470485	0.4526455	0.4575653
0.150	0.3688740	0.3734923	0.3775518
0.175	0.2906995	0.2943391	0.2975382
0.200	0.2125250	0.2151858	0.2175247
0.225	0.1707000	0.1728372	0.1747157
0.250	0.1288750	0.1304885	0.1319068
0.275	0.0870500	0.0881399	0.0890979
0.300	0.0452542	0.0458208	0.0463188
0.325	0.0352543	0.0356957	0.0360836
0.350	0.0252544	0.0255705	0.0258485
0.375	0.0152544	0.0154454	0.0156133
0.400	0.0052545	0.0053203	0.0053781
0.425	0.0039409	0.0039902	0.0040336
0.450	0.0026273	0.0026601	0.0026891
0.475	0.0013136	0.0013301	0.0013445
0.500	0.0000000	0.0000000	0.0000000
0.525	-0.0013136	-0.0013301	-0.0013445
0.550	-0.0026273	-0.0026601	-0.0026891
0.575	-0.0039409	-0.0039902	-0.0040336
0.600	-0.0052545	-0.0053203	-0.0053781
0.625	-0.0152544	-0.0154454	-0.0156133
0.650	-0.0252544	-0.0255705	-0.0258485
0.675	-0.0352543	-0.0356957	-0.0360836
0.700	-0.0452542	-0.0458208	-0.0463188
0.725	-0.0870500	-0.0881399	-0.0890979
0.750	-0.1288750	-0.1304885	-0.1319068
0.775	-0.1707000	-0.1728372	-0.1747157
0.800	-0.2125250	-0.2151858	-0.2175247
0.825	-0.2906995	-0.2943391	-0.2975382
0.850	-0.3688740	-0.3734923	-0.3775518
0.875	-0.4470485	-0.4526455	-0.4575653
0.900	-0.5252230	-0.5317988	-0.5375789
0.925	-0.3939173	-0.3988491	-0.4031842
0.950	-0.2626115	-0.2658994	-0.2687894
0.975	-0.1313058	-0.1329497	-0.1343947
1.000	0.0000000	0.0000000	0.0000000

at external layer (z= h/2). Generally, an anti-symmetric behavior is observed for axial displacement.

In continuation, the effect of various distributions of graphene is studied on the results of composite sandwich panel. Tables 3 and 4 highlight variation in radial displacement U_z and axial displacement U_x along the x direction for two distributions ($U - W_{Gr}$, $X - W_{Gr}$), respectively. The maximum radial and axial displacements is occurred for

Table 9 Longitudinal variation of radial displacement $\boldsymbol{U_z}$ for porosity coefficients

$\%\mathbf{W}_{gr}$	e_0=0.1	e_0=0.3	e_0=0.5
0.0	4.6122520	5.0135179	5.4562941
0.1	4.5722521	4.9700380	5.4089742
0.2	4.5322522	4.9265581	5.3616543
0.3	4.4922522	4.8830782	5.3143344
0.4	4.4522523	4.8395983	5.2670145
0.5	4.4122524	4.7961184	5.2196946
0.6	4.4002527	4.7830747	5.2054990
0.7	4.3882530	4.7700311	5.1913033
0.8	4.3762534	4.7569874	5.1771077
0.9	4.3642537	4.7439438	5.1629121
1.0	4.3522541	4.7309002	5.1487166
1.1	4.3163158	4.6918353	5.1062016
1.2	4.2803775	4.6527703	5.0636866
1.3	4.2444392	4.6137054	5.0211716
1.4	4.2085009	4.5746405	4.9786566
1.5	4.1725625	4.5355754	4.9361414
1.6	4.1405571	4.5007855	4.8982790
1.7	4.1085517	4.4659957	4.8604166
1.8	4.0765462	4.4312058	4.8225542
1.9	4.0445408	4.3964159	4.7846918
2.0	4.0125354	4.3616260	4.7468294
2.1	4.0025373	4.3507581	4.7350016
2.2	3.9925392	4.3398902	4.7231739
2.3	3.9825412	4.3290222	4.7113462
2.4	3.9725431	4.3181543	4.6995185
2.5	3.9625450	4.3072864	4.6876907
2.6	3.9525469	4.2964185	4.6758630
2.7	3.9425488	4.2855506	4.6640353
2.8	3.9325508	4.2746827	4.6522075
2.9	3.9225527	4.2638148	4.6403798
3.0	3.9125546	4.2529469	4.6285521

Table 10 Longitudinal variation of radial displacement $\boldsymbol{U_z}$ for porosity coefficients

$\%\mathbf{W}_{gr}$	e_0=0.1	e_0=0.3	e_0=0.5
0.0	3.5022540	3.8069501	4.1431665
0.1	3.4203112	3.7178783	4.0462281
0.2	3.3383684	3.6288065	3.9492898
0.3	3.2564256	3.5397346	3.8523515
0.4	3.1744828	3.4506628	3.7554132
0.5	3.0925240	3.3615736	3.6584559
0.6	2.9511811	3.2079338	3.4912472
0.7	2.8098382	3.0542941	3.3240385
0.8	2.6684952	2.9006543	3.1568299
0.9	2.5271523	2.7470146	2.9896212
1.0	2.3858254	2.5933922	2.8224314
1.1	2.2444825	2.4397525	2.6552228
1.2	2.1031396	2.2861127	2.4880141
1.3	1.9617966	2.1324729	2.3208054
1.4	1.8204537	1.9788332	2.1535968
1.5	1.7685824	1.9224491	2.0922330
1.6	1.7140315	1.8631522	2.0276992
1.7	1.6594806	1.8038554	1.9631655
1.8	1.6049296	1.7445585	1.8986318
1.9	1.5503787	1.6852617	1.8340980
2.0	1.4958254	1.6259622	1.7695614
2.1	1.4412745	1.5666654	1.7050277
2.2	1.3867236	1.5073685	1.6404940
2.3	1.3321726	1.4480717	1.5759602
2.4	1.2776217	1.3887748	1.5114265
2.5	1.2012542	1.3057633	1.4210837
2.6	1.1467033	1.2464665	1.3565500
2.7	1.0921524	1.1871696	1.2920162
2.8	1.0376014	1.1278728	1.2274825
2.9	0.9830505	1.0685759	1.1629488
3.0	0.9284996	1.0092791	1.0984150

distribution $U - W_{Gr}$ where the minimum structural stiffness is occurred.

The effect of N_L of graphene is investigated on the results of the composite panel. Tables 5 and 6 show variation in radial U_z and axial U_x displacements along x direction for various $N_L = 2,3,4,5$, respectively. It is concluded an enhancement in N_L leads to a diminish in radial and axial displacements.

Tables 7 and 8 investigates impact of various thermal loading $\Delta T = 50,100,150$ on the variation in radial U_z and axial U_x displacements along the x direction, respectively. An enhancement in both radial and axial displacements is observed with an increase in temperature rising because of a decrease in stiffness and increase in thermal strain.

As an important conclusion, the effect of W_{Gr} and porosity coefficient of porous core e_0 is studied on the deformation analysis of sandwich composite cylindrical panel. Tables 9 and 10 investigate variation in radial U_z and axial U_x displacements in terms of W_{Gr} for various $e_0 = 0.2, 0.4, 0.6$, respectively. A significant decrease in absolute value of U_z and U_x is observed with an increase in the fraction of graphene W_{Gr} because of an increase in stiffness. Furthermore, an enhancement in both deflections is observed with an increase in porosity coefficients e_0 because of a decrease in stiffness.

Tables 11 and 12 show variation in radial displacement U_z and axial displacement U_x along x for various distribution of porosity (Monotonous, Symmetric and Nonsymmetric), respectively. The results incicates that the maximum and minimum displacements are obtained for Monotonous and Symmetric distributions, respectively.

Table 11 Longitudinal variation of radial displacement U_z for various distributions of porosity

x/L	Monotonous	Nonsymmetric	Symmetric
0	0.0000000	0.0000000	0.0000000
0.025	0.5033125	0.4303322	0.4250474
0.050	1.0066250	0.8606644	0.8500948
0.075	1.5099375	1.2909966	1.2751422
0.100	2.0132500	1.7213288	1.7001896
0.125	2.3837500	2.0381063	2.0130769
0.150	2.7542500	2.3548838	2.3259641
0.175	3.1247500	2.6716613	2.6388514
0.200	3.4952500	2.9884388	2.9517386
0.225	3.5855825	3.0656730	3.0280244
0.250	3.6759150	3.1429073	3.1043102
0.275	3.7662475	3.2201416	3.1805960
0.300	3.8565800	3.2973759	3.2568818
0.325	3.8567475	3.2975191	3.2570233
0.350	3.8569150	3.2976623	3.2571647
0.375	3.8570825	3.2978055	3.2573062
0.400	3.8572500	3.2979488	3.2574476
0.425	3.8835728	3.3204547	3.2796772
0.450	3.9098955	3.3429607	3.3019067
0.475	3.9362183	3.3654666	3.3241363
0.500	3.9625410	3.3879726	3.3463659
0.525	3.9362183	3.3654666	3.3241363
0.550	3.9098955	3.3429607	3.3019067
0.575	3.8835728	3.3204547	3.2796772
0.600	3.8572500	3.2979488	3.2574476
0.625	3.8570825	3.2978055	3.2573062
0.650	3.8569150	3.2976623	3.2571647
0.675	3.8567475	3.2975191	3.2570233
0.700	3.8565800	3.2973759	3.2568818
0.725	3.7662475	3.2201416	3.1805960
0.750	3.6759150	3.1429073	3.1043102
0.775	3.5855825	3.0656730	3.0280244
0.800	3.4952500	2.9884388	2.9517386
0.825	3.1247500	2.6716613	2.6388514
0.850	2.7542500	2.3548838	2.3259641
0.875	2.3837500	2.0381063	2.0130769
0.900	2.0132500	1.7213288	1.7001896
0.925	1.5099375	1.2909966	1.2751422
0.950	1.0066250	0.8606644	0.8500948
0.975	0.5033125	0.4303322	0.4250474
1.000	0.0000000	0.0000000	0.0000000

Table 12 Longitudinal variation of radial displacement U_z for various distributions of porosity

x/L	Monotonous	Nonsymmetric	Symmetric
0	0.0000000	0.0000000	0.0000000
0.025	0.1313058	0.1276948	0.1227971
0.050	0.2626115	0.2553897	0.2455943
0.075	0.3939173	0.3830845	0.3683914
0.100	0.5252230	0.5107794	0.4911885
0.125	0.4470485	0.4347547	0.4180798
0.150	0.3688740	0.3587300	0.3449710
0.175	0.2906995	0.2827053	0.2718622
0.200	0.2125250	0.2066806	0.1987534
0.225	0.1707000	0.1660058	0.1596386
0.250	0.1288750	0.1253309	0.1205239
0.275	0.0870500	0.0846561	0.0814092
0.300	0.0452542	0.0440097	0.0423217
0.325	0.0352543	0.0342848	0.0329698
0.350	0.0252544	0.0245599	0.0236179
0.375	0.0152544	0.0148349	0.0142659
0.400	0.0052545	0.0051100	0.0049140
0.425	0.0039409	0.0038325	0.0036855
0.450	0.0026273	0.0025550	0.0024570
0.475	0.0013136	0.0012775	0.0012285
0.500	0.0000000	0.0000000	0.0000000
0.525	-0.0013136	-0.0012775	-0.0012285
0.550	-0.0026273	-0.0025550	-0.0024570
0.575	-0.0039409	-0.0038325	-0.0036855
0.600	-0.0052545	-0.0051100	-0.0049140
0.625	-0.0152544	-0.0148349	-0.0142659
0.650	-0.0252544	-0.0245599	-0.0236179
0.675	-0.0352543	-0.0342848	-0.0329698
0.700	-0.0452542	-0.0440097	-0.0423217
0.725	-0.0870500	-0.0846561	-0.0814092
0.750	-0.1288750	-0.1253309	-0.1205239
0.775	-0.1707000	-0.1660058	-0.1596386
0.800	-0.2125250	-0.2066806	-0.1987534
0.825	-0.2906995	-0.2827053	-0.2718622
0.850	-0.3688740	-0.3587300	-0.3449710
0.875	-0.4470485	-0.4347547	-0.4180798
0.900	-0.5252230	-0.5107794	-0.4911885
0.925	-0.3939173	-0.3830845	-0.3683914
0.950	-0.2626115	-0.2553897	-0.2455943
0.975	-0.1313058	-0.1276948	-0.1227971
1.000	0.0000000	0.0000000	0.0000000

5. Conclusions

The higher-order mathematical modeling was developed in this paper in order present deformation analysis of a sandwich cylindrical panel manufactured from porous core with different functionalities sandwiched by two copper matrix reinforced with graphene origami. The constitutive relations were extended in the cylindrical coordinate using the effective material properties reported from the experimental results. The governing equations were derived

using the virtual work principle and the resulting equations were solved using the Eigenvalue-Eigenvector method for clamped boundary conditions. The main conclusions of this paper are expressed as follows:

Investigating the impact of porosity coefficient of porous core indicates that the structural stiffness is decreased that leads to an increase in displacement components.

The foldability parameter has significant in change of modulus of elasticity, where a significant decrease in structural stiffness is observed that leads to an increase in deformation of the structures.

The graphene origami amount has an increasing effect on the stiffness of the reinforced structure that leads to a decrease in deformation of the structures.

Investigating effect of volume fraction of graphene indicates that one can arrive at a decrease in axial and radial displacements with an enhancement in this parameter.

An increase in radial displacement and a decrease in axial displacement is deduced with an increase in porosity coefficient because of a decrease in stiffness.

To investigated impact of the thickness of each core and attachment layers, for the total thickness, it is concluded that the radial displacement is magnified with an increase in core to layers' thickness ratio.

Investigating the effect of span angle on the deformation analysis leads to a decrease in stiffness of the panel and consequently an increase in deformation components.

Acknowledgement

The authors extend their appreciation to the Deanship of Research and Graduate Studies at King Khalid University for funding this work through Large Research Project under grant number RGP2/40/45.

References

Adab, N. and Arefi, M. (2022), "Vibrational behavior of truncated conical porous GPL-reinforced sandwich micro/nano-shell", *Eng. Comput.*, **39**, 419-433. https://doi.org/10.1007/s00366-021-01580-8.

Adab, N., Arefi, M. and Amabili, M. (2022), "A comprehensive vibration analysis of rotating truncated sandwich conical microshells including porous core and GPL-reinforced face-sheets", *Compos. Struct.*, **279**, 114761. https://doi.org/10.1016/j.compstruct.2021.114761

Armenakas, A.E., Gazis, D.C. and Herrmann, G. (2013), *Free Vibrations of Circular Cylindrical Shells, 1st edition*, Pergamon, U.K.

An, J., Wang, A., Zhang, K., Zhang, W., Song, L., Xiao, B. and Wang, R. (2023), "Bending and buckling analysis of functionally graded graphene origami metamaterial irregular plates using generalized finite difference method", *Results. Phys.*, **53**, 106945. https://doi.org/10.1016/j.rinp.2023.106945

Araki, K. and Zhang, R.Z. (2020), "Plasmon-resonance emission tailoring of "origami" graphene-covered photonic gratings", *Opt. Exp.*, **28**(15), 22791-22802. https://doi.org/10.1364/OE.397501

Araki, K. and Zhang, R.Z. (2021), "Tailoring optical properties of "origami" graphene-covered photonic gratings", *IEEE. Phot. Conf.* (IPC), Vancouver, BC, Canada, 1-2. https://doi.org/10.1109/IPC48725.2021.9593055.

Arefi, M., Faegh, R.K. and Loghman, A. (2016), "The effect of axially variable thermal and mechanical loads on the 2D thermoelastic response of FG cylindrical shell", *J. Therm. Stress.*, **39**, 12, 1539-1559. https://doi.org/10.1080/01495739.2016.1217178.

Arefi, M. Mohammad-Rezaei Bidgoli E. Zenkour, A.M. (2019), "Free vibration analysis of a sandwich nano-plate including FG core and piezoelectric face-sheets by considering neutral surface", *Mech. Adv. Mater. Struct.*, **26**, 9, 741-752. https://doi.org/10.1080/15376494.2018.1455939

Arefi, M., Moghaddam, S.K., Bidgoli, E.M.R., Kiani, M. and Civalek, O. (2021), "Analysis of graphene nanoplatelet reinforced cylindrical shell subjected to thermo-mechanical loads", *Compos. Struct.*, **255**, 1, 112924. https://doi.org/10.1016/j.compstruct.2020.112924.

Arefi, M. and Rahimi, G.H. (2011), "Non linear analysis of a functionally graded square plate with two smart layers as sensor and actuator under normal pressure", *Smart. Struct. Syst.*, **8**(5), 433-447. https://doi.org/10.12989/sss.2011.8.5.433

Arefi, M. and Rahimi, G.H. (2012a), "The effect of nonhomogeneity and end supports on the thermo elastic behavior of a clamped–clamped FG cylinder under mechanical and thermal loads", *Int. J. Press. Ves. Pip.*, **96-97**, 30-37. https://doi.org/10.1016/j.ijpvp.2012.05.009

Arefi, M. and Rahimi, G.H. (2012b), "Three-dimensional multi-field equations of a functionally graded piezoelectric thick shell with variable thickness, curvature and arbitrary nonhomogeneity", *Acta. Mech.*, **223**, 63-79. https://doi.org/10.1007/s00707-011-0536-5

Arefi, M. and Rahimi, G.H. (2012c), "Studying the nonlinear behavior of the functionally graded annular plates with piezoelectric layers as a sensor and actuator under normal pressure", *Smart. Struct. Syst.*, **9**(2), 127-143. https://doi.org/10.12989/sss.2012.9.2.127.

Arefi, M. (2020), "Size-dependent electro-elastic analysis of a three-layered piezoelectric doubly curved nano shell", *Mech. Adv. Mater. Struct.*, **27**(23), 1945-1965. https://doi.org/10.1080/15376494.2018.1533605

Arefi, M. (2018), "Nonlocal free vibration analysis of a doubly curved piezoelectric nano shell", *Steel. Compos. Struct.*, **27**(4), 479-493. https://doi.org/10.12989/scs.2018.27.4.479

Arefi, M. and Zenkour, A.M. (2017), "Thermo-electro-magneto-mechanical bending behavior of size-dependent sandwich piezomagnetic nanoplates", *Mech. Res. Com.*, **84**, 27-42. https://doi.org/10.1016/j.mechrescom.2017.06.002

Arefi, M. and Zenkour, A.M (2018), "Free vibration analysis of a three-layered microbeam based on strain gradient theory and three-unknown shear and normal deformation theory", *Steel. Compos. Struct.*, **26**(4), 421-437. https://doi.org/10.12989/scs.2018.26.4.421

Arefi, M. and Zenkour, A.M. (2019), "Influence of micro-length-scale parameters and inhomogeneities on the bending, free vibration and wave propagation analyses of a FG Timoshenko's sandwich piezoelectric microbeam", *J. Sandw. Struct. Mater.*, **21**(4), 1243-1270. https://doi.org/10.1177/1099636217714181.

Arefi, M. and Mohammad-Rezaei Bidgoli, E. (2019), "Electro-elastic displacement and stress analysis of the piezoelectric doubly curved shells resting on Winkler's foundation subjected to applied voltage", *Mech. Adv. Mater. Struct.*, **26**(23), 1981-1994. https://doi.org/10.1080/15376494.2018.1455937

Bai, B. Xu, T. Nie, Q. Li, P. (2020), "Temperature-driven migration of heavy metal Pb2+ along with moisture movement in unsaturated soils", *Int. J. Heat. Mass. Transf.*, **153**, 119573. https://doi.org/10.1016/j.ijheatmasstransfer.2020.119573.

Bai, B. Bai, F. Li, X. Nie, Q. Jia. X. (2022), "The remediation

efficiency of heavy metal pollutants in water by industrial red mud particle waste", *Environ. Tech. Innov.*, **28**, 102944. https://doi.org/10.1016/j.eti.2022.102944.

Bai, B., Bai, F., Nie, Q. and Jia, X. (2023), "A high-strength red mud–fly ash geopolymer and the implications of curing temperature", *Powder Tech.*, **416**, 118242. https://doi.org/10.1016/j.powtec.2023.118242.

Bai, B., Chen, J., Bai, F., Nie, Q. and Jia, X. (2024a), "Corrosion effect of acid/alkali on cementitious red mud-fly ash materials containing heavy metal residues", *Environ. Tech. Innov.*, **33**, 103485. https://doi.org/10.1016/j.eti.2023.103485.

Bai B., Chen J., Zhang B., Chen L. and Zong Y. (2024b), "The solidification of heavy metal Pb2+-contaminated soil by enzyme-induced calcium carbonate precipitation combined with biochar", *Biochem. Eng. J.*, **212**, 109496. https://doi.org/10.1016/j.bej.2024.109496

Bai, B. Chen, J. Zhang, B. and Wang, H. (2024C), "Migration trajectories and blocking effect of the fine particles in porous media based on particle flow simulation", *AIP. Adv.*, **14**, 045036. http://doi.org/10.1063/5.0199046

Bao, X.J., Li, J., Shen, X., Chen, C., Zhang, H. and Cui, H. (2025), "Comprehensive multivariate joint distribution model for marine soft soil based on the vine copula", *Comput. Geotech.*, **177A**, 106814. https://doi.org/10.1016/j.compgeo.2024.106814

Costa, A.T. Ferreira, M.S. Hallam, T. Duesberg G.S. Castro Neto, A.H. (2013), "Origami-based spintronics in graphene", *Europhys. Lett.*, **104**, 47001. https://doi.org/10.12989/eul.2023.14.5.443

Chen, X., Yang, P., Peng, Y., Wang, M., Hu, F. and Xu, J. (2023), "Output voltage drop and input current ripple suppression for the pulse load power supply using virtual multiple quasi-notch-filters impedance", *IEEE. T Power. Electr.*, **38**(8), 9552-9565. https://doi.org/10.1109/TPEL.2023.3275304.

Chen, Q., Mei, X., He, J., Yang, J. and Liu, K. (2024), "Modeling and compensation of small-sample thermal error in precision machine tool spindles using spatial–temporal feature interaction fusion network", *Adv. Eng. Inform.*, **62B**, 102741. https://doi.org/10.1016/j.aei.2024.102741

Cheng, X., Pan, Z., Fan, C., Wu, Z., Ding, L. and Peng, L.M. (2024) "Aligned carbon nanotube–based electronics on glass wafer", *Sci. Adv.*, **10**(12), eadl1636. https://doi.org/10.1126/sciadv.adl1636.

Dai, Y., Jiang, Z., Chen, K.Y., Zuo, D., Ali, H. E. and Albaijan, I. (2023), "Geometry impact on the stability behavior of cylindrical microstructures: Computer modeling and application for small-scale sport structures", *Steel. Compos. Struct.*, **48**(4), 443-459. https://doi.org/10.12989/scs.2023.48.4.443.

Din, Q., Ishaque, W., Maqsood, I. and Tounsi, A. (2023), "Discretization of laser model with bifurcation analysis and chaos control", *Adv. Nano. Res.* **15**(1), 25-34. https://doi.org/10.12989/anr.2023.15.1.025.

Dai, Z., Jiang, Z. and Zhang, L. and Habibi, M. (2021), "Frequency characteristics and sensitivity analysis of a size-dependent laminated nanoshell", *Adv. Nano. Res.*, **10**(2), 175-189. https://doi.org/10.12989/anr.2021.10.2.175.

Du, S., Yin, J., Xie, H., Sun, Y., Fang, T., Wang, Y. and Zheng, R. (2022), "Auger scattering dynamic of photo-excited hot carriers in nano-graphite film", *Appl. Phys. Let.*, **121**(18), 181104. https://doi.org/10.1063/5.0116720.

Dong, J.F., Guan, Z.W., Chai, H.K. and Wang, Q.Y. (2023), "High temperature behaviour of basalt fibre-steel tube reinforced concrete columns with recycled aggregates under monotonous and fatigue loading", *Constr. Build. Mater.*, **389**, 131737. https://doi.org/10.1016/j.conbuildmat.2023.131737.

Dong, J., Liu, Y., Yuan, S., Li, K., Zhang, F., Guan, Z., Chai, H.K. and Wang, Q. (2024), "Mechanical behavior and impact resistance of rubberized concrete enhanced by basalt fiber-epoxy resin composite", *Constr. Build. Mater.*, **435**, 136836. https://doi.org/10.1016/j.conbuildmat.2024.136836.

Fan, J., Pan, Y., Wang, H. and Song, F. (2024a), "Efficient reverse osmosis-based desalination using functionalized graphene oxide nanopores", *Appl. Surf. Sci.*, **674**, 160937. https://doi.org/10.1016/j.apsusc.2024.160937.

Fan, J., Zhang, X., He, N. and Song, F. and Zhang, X. (2024b), "Physical absorption and thermodynamic modeling of CO2 in new deep eutectic solvents", *J. Mole. Liq.*, **402**,124752. https://doi.org/10.1016/j.molliq.2024.124752

Fu, T., Hu, X. and Yang, C. (2023). "Impact response analysis of stiffened sandwich functionally graded porous materials doubly-curved shell with re-entrant honeycomb auxetic core", *Appl. Math. Modell.*, **124**, 553-575. https://doi.org/10.1016/j.apm.2023.08.024

Feng, G., Xie, W., Jiang, F., Yang, Q., Jin, W., Shao, C., Yu, J., Wu, Q., Wang, D. and Liu, J. (2024), "Effects of cores types on non-solvent displacement nonaqueous precipitation synthesis of core-shell structured materials: A case study on effects of carbon sources on C@ZrSiO4 preparation", *Ceram. Int.*, **50**, 11, A, 18370-18379. https://doi.org/10.1016/j.ceramint.2024.02.321.

Guo, H., Zhuang, X. and Rabczuk, T. (2019). "A deep collocation method for the bending analysis of kirchhoff plate", *Comput. Mater. Continua.*, **59**(2), 433-456. https://doi.org/10.32604/cmc.2019.06660

Guo, J., Liu, Y., Zou, Q., Ye, L., Zhu, S. and Zhang, H. (2023), "Study on optimization and combination strategy of multiple daily runoff prediction models coupled with physical mechanism and LSTM", *J. Hydrol.*, **624**, 129969. https://doi.org/10.1016/j.jhydrol.2023.129969

Guo, S., Zuo, X., Wu, W., Yang, X., Zhang, J., Li, Y., Huang, C., Bu, J. and Zhu, S. (2024), "Mitigation of tropospheric delay induced errors in TS-InSAR ground deformation monitoring", *Int. J. Digital. Earth.*, **17**(1). ttps://doi.org/10.1080/17538947.2024.2316107

Ho, D.T., Park, H.S., Kim, S.Y. and Schwingenschlögl, U. (2020), "Graphene origami with highly tunable coefficient of thermal expansion", *ACS Nano*, **14**(7), 8969-8974. https://doi.org/10.1021/acsnano.0c03791

Hong, S., Shi, Y., Li, R., Zhang, C., Jin, Y. and Wang, P. (2018), "Nature-inspired, 3D origami solar steam generator toward near full utilization of solar energy", *ACS. Appl. Mater. Interf.*, **10**(34), 28517-28524. https://doi.org/10.1021/acsami.8b07150

Ho, D.T., Kim, S.Y. and Schwingenschlögl, U. (2020), "Graphene origami structures with superflexibility and highly tunable auxeticity", *Phys. Rev. B.*, **102**(17), 174106. https://doi.org/10.1103/PhysRevB.102.174106.

Huang, X., Chang, L., Zhao, H. and Cai, Z. (2022), "Study on craniocerebral dynamics response and helmet protective performance under the blast waves", *Mater. Des.*, **224**, 111408. https://doi.org/10.1016/j.matdes.2022.111408

Huang, Z., Li, K., Jiang, Y., Jia, Z., Lv, L. and Ma, Y. (2024a), "Graph Relearn Network: Reducing performance variance and improving prediction accuracy of graph neural networks", *Knowl. Based Syst.*, **301**, 112311. https://doi.org/10.1016/j.knosys.2024.112311

Huang, B., Kang, F., Li, X. and Zhu, S. (2024b), "Underwater dam crack image generation based on unsupervised image-to-image translation", *Automat. Constr.*, **163**, 105430. https://doi.org/10.1016/j.autcon.2024.105430

Hu, Y., Zhang, X.C., Wang, G.Q., Zhang, X.P. and Li, H.Z. (2024), "Hovering efficiency optimization of ducted propeller with large blade tip clearance based on grooved duct configuration", *Aeros. Sci. Tech.*, **150**, 109226. https://doi.org/10.1016/j.ast.2024.109226.

Hui, M., Jia, X., Li, X., Lazcano-Silveira, R. abd Shi, M. (2023), "Anti-inflammatory and antioxidant effects of liposoluble C60 at the cellular, molecular, and whole-animal levels", *J. Inflam.*

Res., **16**, 83-93. https://doi.org/10.2147/JIR.S386381

Jia, G., Luo, J., Cui, C., Kou, R., Tian, Y. and Schubert, M. (2024), "Valley quantum interference modulated by hyperbolic shear polaritons", *Phys. Rev. B*, **109**, 155417. https://doi.org/10.1103/PhysRevB.109.155417.

Jiang, X., Wang, Y., Zhao, D. and Shi, L. (2024), "Online Pareto optimal control of mean-field stochastic multi-player systems using policy iteration", *Sci. China. Inf. Sci.*, **67**, 140202. https://doi.org/10.1007/s11432-023-3982-y

Jing, C., Bing, B. and Qiang. D. (2024), "Durability evaluation of a high-performance red mud-based composite material", *Mater. Today. Com.*, **39**, 108684. https://doi.org/10.1016/j.mtcomm.2024.108684

Kuang, W., Wang, H., Li, X., Zhang, J., Zhou, Q. and Zhao, Y. (2018), "Application of the thermodynamic extremal principle to diffusion-controlled phase transformations in Fe-C-X alloys: Modeling and applications", *Acta. Mater.*, **159**, 16-30. https://doi.org/10.1016/j.actamat.2018.08.008

Kadiri, A., Bendaida, M., Attia, A., Balubaid, M., Mahmoud, S.R., Bousahla, A.A. and Tounsi, A. (2024), "Wave propagation in FG polymer composite nanoplates embedded in variable elastic medium", *Adv. Nano. Res.*, **17**(3), 235-248. https://doi.org/10.12989/anr.2024.17.3.235

Kumar, Y., Gupta, A. and Tounsi, A. (2021) "Size-dependent vibration response of porous graded nanostructure with FEM and nonlocal continuum model", *Adv. Nano. Res.*, **11**(1), 1-17. https://doi.org/10.12989/anr.2021.11.1.001.

Lori Dehsaraji, M., Arefi, M. and Loghman, A. (2021), "Size dependent free vibration analysis of functionally graded piezoelectric micro/nano shell based on modified couple stress theory with considering thickness stretching effect", *Def. Tech.*, **17**(1),119-134. https://doi.org/10.1016/j.dt.2020.01.001.

Lv, C., Krishnaraju, D., Konjevod, G., Yu, H. and Jiang, H. (2014), "Origami based Mechanical Metamaterials", *Sci. Rep.*, **4**, 5979. https://doi.org/10.1038/srep05979

Li, J., Wang, Z., Zhang, S., Lin, Y., Wang, L., Sun, C. and Tan, J. (2023), "A novelty mandrel supported thin-wall tube bending cross-section quality analysis: A diameter-adjustable multi-point contact mandrel", *Int. J. Adv. Manuf. Tech.*, **124**(11), 4615-4637. https://doi.org/10.1007/s00170-023-10838-y

Li, F., Gan, J., Zhang, L., Tan, H., Li, E. and Li, B. (2024a). "Enhancing impact resistance of hybrid structures designed with triply periodic minimal surfaces", *Compos. Sci. Tech.*, **245**, 110365. https://doi.org/10.1016/j.compscitech.2023.110365

Li, J., Yang, H., Gu, X., Zou, Y., Zhan, D. and Peng, J. (2024b), "Recent advances in scanning electrochemical microscopy for probing the sites in electrocatalysts", *J. Mater. Chemistry. A.* **12**(30), 18733-18750. http://doi.org/10.1039/D4TA01292E

Lei, M., Wan, H., Song, J., Lu, Y., Chang, R., Wang, H., Zhou, H., Zhang, X., Liy, C, and Qu, X. (2024), "Programmable electro-assembly of collagen: constructing porous janus films with customized dual signals for immunomodulation and tissue regeneration in periodontitis treatment", *Adv. Sci.*, **11**(13), 2305756. https://doi.org/10.1002/advs.202305756.

Liang, K., Sun, P. and Wang, D. (2024). "Quantitative analysis of deformation performance for skew slab based on deformation energy decomposition method of triangular prism element", *Structures*, **63**, 106447. https://doi.org/10.1016/j.istruc.2024.106447

Lu, Y., Guo, Z., Zhang, M., Jiang, X. and Wang, X. (2025), "Flow-heat coupling analysis of the 1/4 symmetrical CAP1400 nuclear island loop based on the source term approach", *Annals. Nucl. Energy.*, **211**, 110926. https://doi.org/10.1016/j.anucene.2024.110926.

Liu, W., Zhao, Y., Zhang, Y., Shuai, C., Chen, L., Huang, Z. and Hou, H. (2023a). "Deformation-induced dynamic precipitation of 14H-LPSO structure and its effect on dynamic recrystallization in hot-extruded Mg-Y-Zn alloys", *Int. J. Plast.*, **164**, 103573. https://doi.org/10.1016/j.ijplas.2023.103573

Liu, J., Liu, T., Su, C. and Zhou, S. (2023b), "Operation analysis and its performance optimizations of the spray dispersion desulfurization tower for the industrial coal-fired boiler", *Case. Stud. Therm. Eng.*, **49**, 103210. https://doi.org/10.1016/j.csite.2023.103210

Liu, Y., Tan, X., Liu, Z., Zeng, E., Mei, J., Jiang, Y., Li, P., Sun, W., Zhao, W., Tian, C., Dong, Y., Xie, Z and Wang, C.A. (2024), "Heat-localized and salt-resistant 3D hierarchical porous ceramic platform for efficient solar-driven interfacial evaporation", *Small*, **20**(34), 2400796. https://doi.org/10.1002/smll.202400796.

Ling, W., Jing, C., Wan, J., Mao, A., Xiao, Q., Guan, J., Cheng, C. and Liu, C. (2024), "Design and construction of the near-earth space plasma simulation system of the Space Plasma Environment Research Facility", *J. Plasma. Phys.*, **90**(1), 345900101. https://doi.org/10.1017/S0022377823001460

Mu, J., Hou, C., Wang, H., Li, Y., Zhang, Q. and Zhu, M. (2015), "Origami-inspired active graphene-based paper for programmable instant self-folding walking devices", *Sci. Adv.*, **1**, 10. https://doi.org/10.1126/sciadv.1500533.

Mohammadi, M., Arefi, M., Dimitri, R. and Tornabene, F. (2019), "Higher-order thermo-elastic analysis of FG-CNTRC cylindrical vessels surrounded by a Pasternak foundation", *Nanomaterials*, **9**(1), 79. https://doi.org/10.3390/nano9010079

Ren, H., Xia, X., Sun, Y., Zhai, Y., Zhang, Z., Wu, J., Li, J. and Liu, M. (2024), "Electrolyte engineering for the mass exfoliation of graphene oxide across wide oxidation degrees", *J. Mater. Chem. A.*, **12**(35), 23416-23424. http://doi.org/10.1039/D4TA02654C

Rui, Z., Bing, B., Guoqing, C. and Xingxin. C. (2024), "Thermo-Hydro-Mechanic-Chemical coupling model for hydrate-bearing sediment within a unified granular thermodynamic theory", *Comput. Geotech.*, **167**, 106057. https://doi.org/10.1016/j.compgeo.2023.106057.

Rahimi, G.H., Arefi, M. and Khoshgoftar, M.J. (2012), "Electro elastic analysis of a pressurized thick-walled functionally graded piezoelectric cylinder using the first order shear deformation theory and energy method", *Mechanika*, **18**(3), 292-300. https://doi.org/10.5755/j01.mech.18.3.1875.

Samaniego, E., Anitescu, C., Goswami, S., Nguyen-Thanh, V.M., Guo, H., Hamdia, K., Zhuang, X. and Rabczuk, T. (2020), "An energy approach to the solution of partial differential equations in computational mechanics via machine learning: Concepts, implementation and applications", *Comput. Meth. Appl. Mech. Eng.*, **362**, 112790. https://doi.org/10.1016/j.cma.2019.112790.

Shenoy, V.B. and Gracias, D.H. (2012), "Self-folding thin-film materials: From nanopolyhedra to graphene origami", *MRS Bull.*, **37**(9), 847-854. https://doi.org/10.1557/mrs.2012.184

Soldatos, K.P. and Hadjigeorgiou, V.P. (1990), "Three-dimensional solution of the free vibration problem of homogeneous isotropic cylindrical shells and panels", *J. Sound Vib.*, **137**(3), 369-384. https://doi.org/10.1016/0022-460X(90)90805-A.

Sekkak, M., Zerrouki, R., Zidour, M., Tounsi, A., Bourada, M., Selim, M.M. and Saad, H.A. (2024) "Static analysis of nonlinear FG-CNT reinforced nano-composite beam resting on Winkler/Pasternak foundation", *Adv. Nano. Res.*, **16**(5), 509-519. https://doi.org/10.12989/anr.2024.16.5.509.

Sun, X., Zhang, K., Liu, Q., Bao, M. and Chen, Y. (2024), "Harnessing domain insights: A prompt knowledge tuning method for aspect-based sentiment analysis", *Knowl. Based Syst.*, **298**, 111975. https://doi.org/10.1016/j.knosys.2024.111975.

Tian, F., Liu, Z., Zhou, J., Chen, L. and Feng, X.T. (2024), "Quantifying post-peak behavior of rocks with Type-I, Type-II,

and mixed fractures by developing a quasi-state-based peridynamics", *Rock. Mech. Rock. Eng*., 1-37. https://doi.org/10.1007/s00603-024-03788-8

Tlidji, Y., Benferhat, R., Daouadji, T.H., Tounsi, A. and Trinh, L. C. (2022), "Free vibration analysis of FGP nanobeams with classical and non-classical boundary conditions using State-space approach", *Adv. Nano. Res*., **13**(5), 453-463. https://doi.org/10.12989/anr.2022.13.5.453.

Wang, Y., Sun, S., Luo, J., Xiong, Y., Ming, T., Liu, J., Ma, Y., Yan, S., Yang, Y., Yang, Z., Reboud, J., Yin, H., Cooper, J.M. and Cai, X. (2020), "Low sample volume origami-paper-based graphene-modified aptasensors for label-free electrochemical detection of cancer biomarker-EGFR", *Microsyst. Nanoeng*., **6**, 32. https://doi.org/10.1038/s41378-020-0146-2

Wang, Z., Zhou, T., Zhang, S., Sun, C., Li, J., Tan, J. (2023), "Bo-LSTM based cross-sectional profile sequence progressive prediction method for metal tube rotate draw bending", *Adv. Eng. Inform.*, **58**, 102152. https://doi.org/10.1016/j.aei.2023.102152

Wang, K., Liu, Z., Wu, M., Wang, C., Shen, W. and Shao, J. (2024a), "Experimental study of mechanical properties of hot dry granite under thermal-mechanical couplings", *Geothermics*, **119**, 102974. https://doi.org/10.1016/j.geothermics.2024.102974

Wang, Y., Du, D., Song, Y., Li, Z., Ye, N., Zhang, Q., Zhang, J., Checn, J. and Cao, B. (2024b), "Photonics-based integrated radar jamming and secure communication system at Ka-Band", *J. Lightwave. Tech.*, **42**(10), 3621-3630. https://doi.org/10.1109/JLT.2024.3362254.

Wei, N., Chen, Y., Zhang, Y., Zheng, J.C., Zhao, J. and Mai, Y.W. (2020), "Crease-induced targeted cutting and folding of graphene origami", *Carbon*, **165**, 259-266. https://doi.org/10.1016/j.carbon.2020.04.058

Wu, Z., Zhang, Y., Zhang, L. and Zheng, H. (2023), "Interaction of cloud dynamics and microphysics during the rapid intensification of super-typhoon Nanmadol (2022) based on multi-satellite observations", *Geophys. Res. Lett*., **50**(15), e2023GL104541. https://doi.org/10.1029/2023GL104541.

Wu, Z., Ma, C., Zhang, L., Gui, H., Liu, J. and Liu, Z. (2024a), "Predicting and compensating for small-sample thermal information data in precision machine tools: A spatial-temporal interactive integration network and digital twin system approach", *Appl. Soft. Comput.*, **161**, 111760. https://doi.org/10.1016/j.asoc.2024.111760

Wu, Y., Kang, F., Zhang, Y., Li, X. and Li, H. (2024b), "Structural identification of concrete dams with ambient vibration based on surrogate-assisted multi-objective salp swarm algorithm", *Structures*, **60**, 105956. https://doi.org/10.1016/j.istruc.2024.105956

Xie, X., Gao, Y., Hou, F., Cheng, T., Hao, A. and Qin, H. (2024), "Fluid inverse volumetric modeling and applications from surface motion", *IEEE. T. Visualiz. Comput. Graph*., **1**(1-17), 5555. https://10.1109/TVCG.2024.3370551

Xie, J., Wen, M., Tu, Y., Wu, D., Liu, K. and Tang, K. (2024b), "Thermal consolidation of layered saturated soil under time-dependent loadings and heating considering interfacial flow contact resistance effect", *Int. J. Numer. Anal. Meth. Geomech*., **48**(5), 1123-1159. https://doi.org/10.1002/nag.3677

Xie, J., Wen, M., Ding, P., Tu, Y., Wu, D., Liu, K., Tang, K. and Chen, M. (2024c), "Interfacial flow contact resistance effect for thermal consolidation of layered viscoelastic saturated soils with semi-permeable boundaries", *Int. J. Numer. Anal. Meth. Geomech*., **48**(15), 3640-3679. https://doi.org/10.1002/nag.3805.

Yang, C., Li, Z., Xu, P., Huang, H. (2024), "Recognition and optimisation method of impact deformation patterns based on point cloud and deep clustering: Applied to thin-walled tubes", *J. Indust. Inform. Integr*., **40**, 100607. https://doi.org/10.1016/j.jii.2024.100607

Yu, L., Lei, Y., Ma, Y., Liu, M., Zheng, J., Dan, D. and Gao, P. (2021), "A comprehensive review of fluorescence correlation spectroscopy", *Front. Phys*., **9**, 644450. https://doi.org/10.3389/fphy.2021.644450.

Yu, X., Feng, B., Yao, M., Peng, J. and Yang, S. (2024a), "Recent progress in modular electrochemical synthesis of hydrogen and high-value-added chemicals based on solid redox mediator", *Small*, 2310573. https://doi.org/10.1002/smll.202310573

Yu, Y., Wan, M., Qian, J., Miao, D., Zhang, Z. and Zhao, P. (2024b), "Feature selection for multi-label learning based on variable-degree multi-granulation decision-theoretic rough sets", *Int. J. Approx. Reason*., **169**, 109181. https://doi.org/10.1016/j.ijar.2024.109181.

Yu, Y., Fu, T., Wang, S. and Yang, C. (2025). "Dynamic response of novel sandwich structures with 3D sinusoid-parallel-hybrid honeycomb auxetic cores: The cores based on negative Poisson's ratio of elastic jump", *Eur. J. Mech. A Solids*, **109**, 105449. https://doi.org/10.1016/j.euromechsol.2024.105449

Zhao, Y., Yan, Y., Jiang, Y., Cao, Y., Wang, Z., Li, J., Yan, C., Wang, D., Yuan, Lu. and Zhao, G. (2024a), "Release pattern of light aromatic hydrocarbons during the biomass roasting process", *Molecules*, **29**, 1188. https://doi.org/10.3390/molecules29061188

Zhao, Y. (2022), "Stability of phase boundary between L12-Ni3Al phases: A phase field study", *Intermetallics*, **144**, 107528. https://doi.org/10.1016/j.intermet.2022.107528.

Zhao, Y., Wang, J., Cao, G., Yuan, Y., Yao, X. and Qi, L. (2023), "Intelligent control of multilegged robot smooth motion: A review", *IEEE Access*, **11**, 86645-86685. https://doi.org/10.1109/ACCESS.2023.3304992.

Zhao, Z., Zhang, H., Shiau, J., Du, W., Ke, L., Wu, F. and Bao, X. (2024b), "Failure envelopes of rigid tripod pile foundation under combined vertical-horizontal-moment loadings in clay", *Appl. Ocean Res*., **150**, 104131. https://doi.org/10.1016/j.apor.2024.104131

Zhen, W., Wang, Z., Wang, Q., Sun, W., Wang, R., Zhang, W., ... & Zhang, H. (2024), "Cardiovascular disease therapeutics via engineered oral microbiota: Applications and perspective", *iMeta*, **3**(3), e197. https://doi.org/10.1002/imt2.197.

Zhan, P., Lou, J. and Chen, T. (2024), "Dynamic hysteresis compensation and iterative learning control for underwater flexible structures actuated by macro fiber composites", *Ocean. Eng*., **298**, 117242. https://doi.org/10.1016/j.oceaneng.2024.117242.

Zhu, J. Ma, B. Li, D. Zhang, Y. and Xu, L. (2024), "Role of bicarbonate in CO2 corrosion of carbon steel", *Electrochimica. Acta*., **478**, 143818, https://doi.org/10.1016/j.electacta.2024.143818.

Zhu, J. and Xiong, J. (2023), "Tunable terahertz graphene metamaterial optical switches and sensors based on plasma-induced transparency", *Measurement*, **220**, 113302. https://doi.org/10.1016/j.measurement.2023.113302.

Zhu, S. and Li, T. (2014), "Hydrogenation-assisted graphene origami and its application in programmable molecular mass uptake, storage, and release", *ACS Nano*, **8**(3), 2864-2872. https://doi.org/10.1021/nn500025t.

Zhang, P. Jia, H. Zhang, Y.F. and Du, S. (2023a), "Atomistic simulations of graphene origami: Dynamics and kinetics", *Chin. Phys. B*., **32**. 087107. https://doi.org/10.1088/1674-1056/acd527

Zhang, T., Deng, F. and Shi, P. (2023b), "Nonfragile Finite-Time Stabilization for Discrete Mean-Field Stochastic Systems", *IEEE. T Automat. Control*, **68**, 10, 6423-6430. https://doi.org/10.1109/TAC.2023.3238849.

Zhang, M., Jiang, X. and Arefi, M. (2023), "Dynamic formulation of a sandwich microshell considering modified couple stress

and thickness-stretching", *Eur. Phys. J. Plus.*, **138**, 227. https://doi.org/10.1140/epjp/s13360-023-03753-4

Zhang, H., Wang, P., Liu, Y., Dai, S., Zhu, Y., Li, B. and Dong, G. (2024a), "Dong, stretch-controlled branch shape microstructures for switchable unidirectional self-driven spreading of oil droplets", *ACS. Appl. Mater. Interf.*, **16**(31), 41694-41703. https://doi.org/10.1021/acsami.4c07736

Zhang, D., Du, C., Peng, Y., Liu, J., Mohammed, S. and Calvi, A. (2024b), "A multi-source dynamic temporal point process model for train delay prediction", *IEEE. T. Intell. Transp. Syst.*, **25**(11), 17865-17877. https://doi.org/10.1109/TITS.2024.3430031.

Zhang, L., Li, D., Liu, P., Liu, X. and Yin, H. (2024c). "The effect of the intensity of withdrawal-motivation emotion on time perception: Evidence based on the five temporal tasks", *Motiv. Sci.*, **10**(2), 138-148. https://doi.org/10.1037/mot0000324

Zhou, C., Zhao, Y., Zhang, J., Fang, Y. and Habibi M., (2020b), "Vibrational characteristics of multi-phase nanocomposite reinforced circular/annular system", *Adv. Nano. Res.*, **9**(4), 295-307. https://doi.org/10.12989/anr.2020.9.4.295

Zhuang, X., Guo, H., Alajlan, N., Zhu, H. and Rabczuk, T. (2021), "Deep autoencoder based energy method for the bending, vibration, and buckling analysis of Kirchhoff plates with transfer learning", *Eur. J. Mech. A Solids*, **87**, 104225. https://doi.org/10.1016/j.euromechsol.2021.104225.

JL